euspen's 25th International Conference & Exhibition, Zaragoza, ES, June 2025
www.euspen.eu

Effects of laser parameters on surface morphology and phase composition in 4H-SiC laser surface modification

Qixian Zhang[1*], Chunjin Wang[1], and Benny C.F. Cheung[1]

[1]*State Key Laboratory of Ultra-precision Machining Technology, Department of Industrial and Systems Engineering, The Hong Kong Polytechnic University, Hung Hom, Kowloon, Hong Kong, China*

qi-xian.zhang@connect.polyu.hk

Abstract
Laser surface modification of 4H-SiC was conducted to investigate the effects of laser processing parameters on ablation depth, surface roughness, surface morphology, and phase composition. The results demonstrate that the femtosecond (FS) laser produces a greater ablation depth and a more pronounced increase in surface roughness compared to the picosecond (PS) laser. In addition to pulse duration, key factors influencing ablation depth and surface roughness include laser power, scanning speed, and scanning interval. The PS laser results in more significant surface oxidation. Both PS and FS lasers lead to the transformation of 4H-SiC into amorphous silicon (a-Si), disordered carbon, and graphite. In contrast to the PS laser, the high-power FS laser significantly reduces the content of disordered carbon and graphite. These effects are primarily attributed to the higher peak energy density of the FS laser, which drives more intensive ablation, and the longer interaction time of the PS laser, which leads to stronger thermal effects. These findings provide valuable insights into the mechanism of laser-SiC interaction and offer a basis for optimizing process parameters in laser surface modification applications.

Silicon carbide (SiC), laser surface modification, laser parameters.

1. Introduction

Silicon carbide (SiC), a representative material of the third generation of semiconductors, shows significant potential in power semiconductor devices due to its wide bandgap, high thermal conductivity, and high breakdown field. However, its high hardness and brittleness substantially challenge achieving efficient and high-quality processing [1].

To overcome these challenges, surface modification techniques that reduce SiC's hardness have been explored, with laser surface modification attracting significant attention for its high efficiency and remarkable effectiveness [2,3]. Liu et al. [4] demonstrated that the hardness of 4H-SiC is significantly reduced after picosecond laser scanning. Chen et al. [5] reported that femtosecond laser scanning induces the formation of laser-induced periodic surface structures (LIPSS) on 4H-SiC surfaces, which reduces scratching forces during nano-scratching and enhances material removal efficiency. Furthermore, Xie et al. [6] and Chen et al. [7] combined laser surface modification with chemical mechanical polishing (CMP), significantly improving material removal rates during CMP. These findings highlight the potential of laser surface modification to enhance SiC processing efficiency. However, although laser surface modification has been widely studied, the extremely short laser action time, the repeated heating and cooling cycles during the laser surface scanning process, and the complex phase transition behavior of SiC collectively result in a highly complex and challenging-to-control evolution of SiC morphology and surface composition under laser irradiation. Therefore, further in-depth investigations into these aspects are necessary to guide parameter selection.

In this study, we investigated the surface modification of 4H-SiC using picosecond and femtosecond lasers, focusing on the effects of laser pulse duration and other parameters on ablation depth, surface roughness, surface morphology, and phase composition.

2. Experimental methods

The n-type 4H-SiC samples (10 × 10 mm) used in this study were laser-cut from sliced 6-inch wafers. A picosecond (PS) laser system with a pulse duration of 15 ps at a wavelength of 1064 nm and a femtosecond (FS) laser system with a pulse duration of 194 fs at a wavelength of 1030 nm were utilized. In addition to pulse duration, parameters such as power, scanning speed, and scanning interval were studied. The Si face of the SiC samples was scanned along a raster path over a 1 × 1 mm area with a laser frequency of 200 kHz. After laser surface scanning, the samples were ultrasonically cleaned in alcohol for 10 minutes and subsequently ultrasonically cleaned in deionized water for 2 minutes to remove oxides and other contaminants.

Ablation depth and surface roughness were measured using white light interferometry (WLI, Zygo NexView). Surface morphology was observed using scanning electron microscopy (SEM, TESCAN MAIA3). Elemental analysis was performed using energy-dispersive X-ray spectroscopy (EDS, Thermo Fisher Scientific Apreo 2). Phase composition was analyzed with Raman spectroscopy (Renishaw Micro-Raman Spectroscopy System).

3. Results and discussion

3.1. Ablation depth and surface roughness

Figure 1(a) presents the ablation depth results for PS and FS lasers at varying powers. As laser power increased from 2 W to 16 W, the ablation depth for the FS laser rose from 5.6 µm to 29.8 µm, while for the PS laser, it increased from 0.7 µm to 3.9 µm. The ablation depths for both lasers showed an almost linear

relationship with increasing power; however, the FS laser consistently achieved significantly greater ablation depths. At the highest power level (16 W), the ablation depth for the FS laser was approximately 7.6 times that of the PS laser. Figure 1(b) shows the arithmetic mean surface roughness (Sa) results for both lasers at varying power levels. The Sa of the original material was approximately 150–200 nm. After laser surface modification, Sa values increased to 220–500 nm. Under identical power conditions, the FS laser produced higher Sa than the PS laser, with differences ranging from 50–250 nm. Additionally, Sa for both lasers generally increased with rising power.

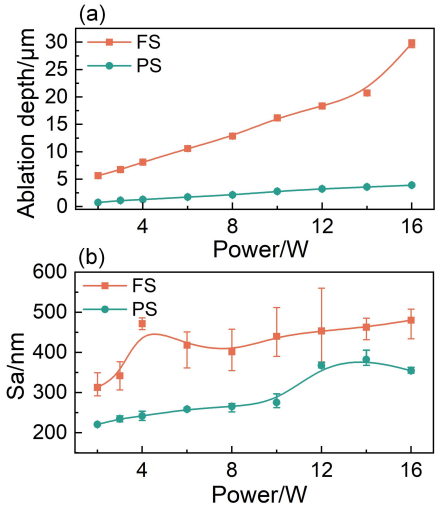

Figure 1. Ablation depth and Sa results under varying powers and pulse durations: (a) ablation depth, and (b) Sa.

Compared with the PS laser, the FS laser concentrates energy over a shorter duration, resulting in a higher peak power density. This leads to a higher maximum temperature and a lower ablation threshold [8]. Consequently, the FS laser produces greater ablation depth and a rougher surface under the same power conditions. Regarding laser power, it directly determines the single-pulse energy. An increase in power and single-pulse energy further raises the surface temperature, thereby enhancing the ablation depth and surface roughness.

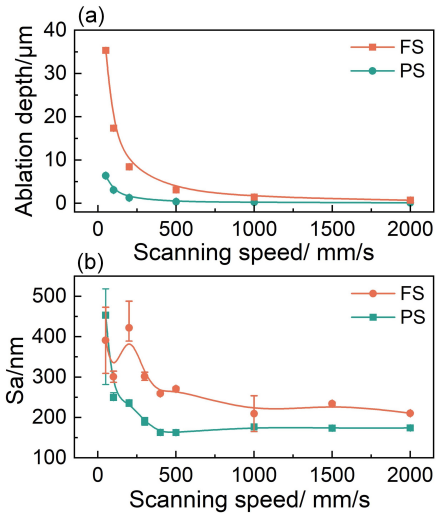

Figure 2. Ablation depth and Sa results under varying scanning speeds and pulse durations: (a) ablation depth, and (b) Sa.

Figure 2(a) presents the ablation depth results for PS and FS lasers at various scanning speeds. As the scanning speed decreased from 2000 mm/s to 20 mm/s, the ablation depth of the FS laser increased significantly, from 0.7 μm to 35.3 μm. Similarly, for the PS laser, the ablation depth rose from 0.12 μm to 6.4 μm with decreasing scanning speed. These results demonstrate that ablation depth increases markedly as scanning speed decreases. Figure 2(b) illustrates the Sa results for PS and FS lasers at different scanning speeds. For the FS laser, Sa exhibited a continuous upward trend, reaching a maximum value of 391 nm. In contrast, for the PS laser, Sa initially decreased slightly, then increased sharply, peaking at 453 nm. Across most scanning speeds, the roughness for PS laser processing was lower than that of FS laser processing, with the exception of very low scanning speeds, where the roughness of PS surpassed that of FS.

A decrease in scanning speed increases the number of pulse irradiations per unit area. At the laser frequency used in this study, although the increased number of pulses does not significantly raise the maximum temperature, it prolongs the duration for which the surface remains in an overheated state [9]. The results in Figure 2 show that this extended overheated state directly influences the ablation depth and surface roughness.

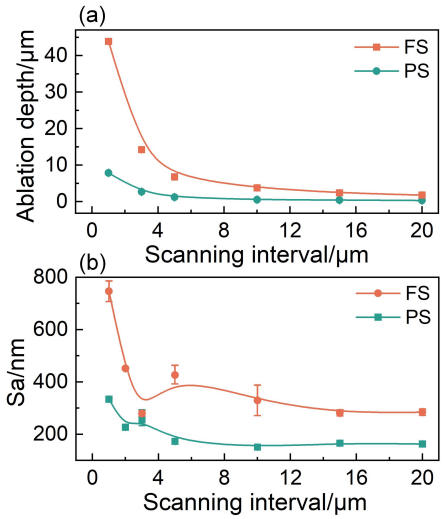

Figure 3. Ablation depth and Sa results under varying scanning intervals and pulse durations: (a) ablation depth, and (b) Sa.

Figure 3(a) displays the ablation depth results for PS and FS lasers at different scanning intervals. When the scanning interval was reduced from 20 μm to 1 μm, the ablation depth of the FS laser increased significantly from 1.8 μm to 43.9 μm. Similarly, for the PS laser, as the scanning interval decreased, the ablation depth rose from 0.3 μm to 7.9 μm. These findings indicate that ablation depth increases notably with decreasing scanning intervals. Figure 3(b) presents the Sa results for PS and FS lasers at varying scanning intervals. For the FS laser, Sa followed a continuous upward trend, reaching a maximum of 746.5 nm. For the PS laser, Sa initially decreased slightly, then increased significantly, peaking at 334 nm. Throughout the range of scanning intervals, the Sa values for PS laser processing consistently remained lower than those for FS laser processing.

Similar to the scanning speed, the scanning interval affects the number of laser irradiations per unit area, and its influence is therefore similar to that of the scanning speed. Additionally, the scanning interval impacts the re-irradiation over a longer period. The effects of scanning speed and scanning interval in this study are comparable, suggesting that at 200 kHz, the thermal effects between pulses on the laser are relatively small.

3.2. Surface morphology

Figure 4 presents the SEM images of laser-modified surfaces, showing the LIPSS [10], which are characteristic features for

both PS and FS lasers. These structures consist of ripples that are oriented perpendicular to the laser polarization direction. For the PS laser, under low power conditions (2 W, Figure 4(a)), the low-spatial frequency LIPSS (LSFL) structure was dominant, with oxide nanoclusters distributed across the LSFL surface. A small amount of high-spatial frequency LIPSS (HSFL) was also present. As the power increased to medium levels (8 W, Figure 4(b)), the LSFL structure almost completely decomposed into HSFL, accompanied by the formation of additional nanocluster oxides. At high power levels (16 W, Figure 4(c)), the LSFL structure re-emerged as the dominant feature but showed partial destruction, with a significant accumulation of nanocluster oxides covering the surface. For the FS laser, at both low and medium power levels (2 W and 8 W, Figure 4(d) and (e)), the LSFL profiles and HSFL structures were clearly observed, with oxides distributed across the surface. However, at high power levels (16 W, Figure 4(f)), HSFL became the predominant surface feature.

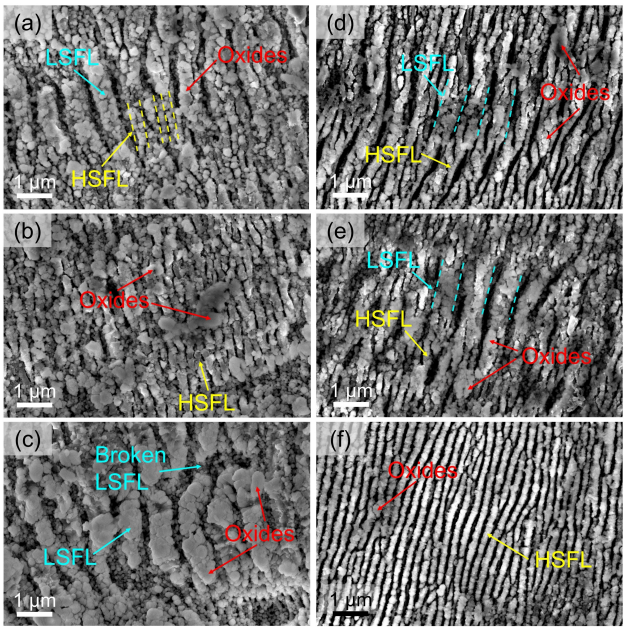

Figure 4. SEM images of laser-modified surfaces: (a) PS-2W, (b) PS-8W, (c) PS-16W, (d) FS-2W, (e) FS-8W, and (f) FS-16W.

The formation mechanism of LIPSS has been extensively explained by electromagnetic theory [10]. Additionally, Chen et al. [5] demonstrated that the structure of LIPSS directly influences the material removal process. This study found that as power increases, the PS laser undergoes an evolution process from LSFL+HSFL to HSFL, and eventually to LSFL+broken LSFL, accompanied by an increase in oxide deposition. In contrast, the FS laser follows an evolution process from LSFL+HSFL to HSFL, with no significant oxide deposition observed. These findings suggest that as power increases, the HSFL becomes more prominent or the LSFL is destroyed, thereby reducing the stiffness of LIPSS, making it easier to break and remove, which in turn enhances the removal efficiency.

3.3. Element composition

Figure 5(a) shows the atomic percentage results for the PS laser under different power levels. As the laser power increased, the silicon (Si) content initially decreased and then fluctuated. The carbon (C) content steadily decreased, while the oxygen (O) content consistently increased. Figure 5(b) illustrates the corresponding results for the FS laser. While the overall trends for Si, C, and O were similar to those observed for the PS laser, the proportion of O in FS-treated surfaces was consistently lower.

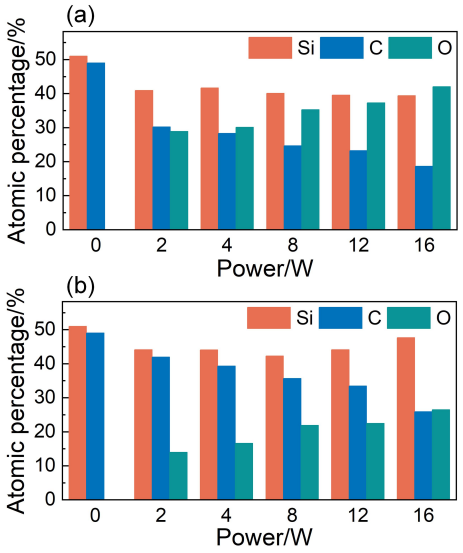

Figure 5. Atomic percentage results under varying powers and pulse durations: (a) PS laser, and (b) FS laser.

Both PS and FS lasers cause significant surface oxidation, with the degree of oxidation increasing as power rises. The oxidation effect is more pronounced with the PS laser, as evidenced by the substantial oxides deposition on the surface of LIPSS in the PS laser, as shown in Figure 4. This is attributed to the longer pulse duration of the PS laser, which results in a longer interaction time between the laser and the material, allowing the surface to remain in an overheated state for a longer period, thereby providing more time for the oxidation reaction. Additionally, the higher single-pulse energy and increased maximum temperature resulting from higher power also promote the oxidation process. In many studies combining laser surface modification and CMP [6,7], it is believed that the formation of Si oxide is the primary reason for the increased material removal rate in CMP. This suggests that the material removal rate of the laser-modified surface in this study will also increase, with the removal rate for the PS laser likely higher than that of the FS laser, and further increasing with power.

3.4. Phase composition

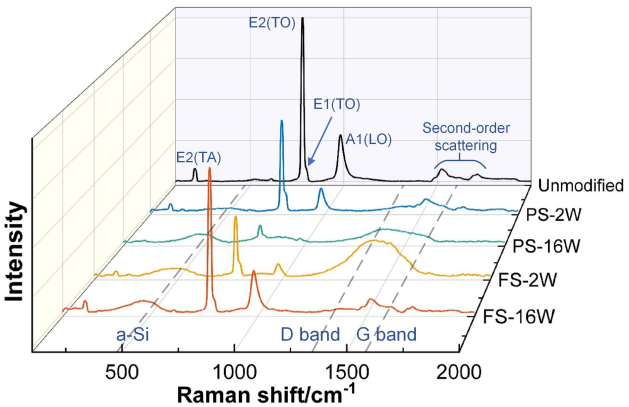

Figure 6. Raman spectra under varying powers and pulse durations.

Figure 6 presents the Raman spectra of unmodified and laser-modified surfaces. For the unmodified 4H-SiC, multiple peaks corresponding to its crystalline structure were observed [11]. Under low-power PS laser conditions (PS-2 W), smaller peaks corresponding to amorphous silicon (a-Si) and D band (disordered carbon) appeared, indicating the initial decomposition of 4H-SiC. At high power levels (PS-16 W), both the a-Si and disordered carbon were significantly enhanced,

along with the appearance of the G band, which corresponds to graphite, suggesting more extensive decomposition with increasing PS power. For the FS laser, under low-power conditions (FS-2 W), rapid decomposition of 4H-SiC into a-Si, disordered carbon, and graphite was observed. As the power increased to high levels (FS-16 W), the a-Si peak persisted, but the intensities of the disordered carbon and graphite were significantly reduced. This indicates that high-power FS laser processing suppresses the formation of disordered carbon and graphite.

Regarding the interaction between FS laser and SiC, Zhang et al. [12] suggested that the formation of the amorphous phase can be ignored. However, this study found that for the FS laser, at lower power, SiC quickly decomposed into a significant amount of the amorphous phase, while at higher power, the amount of amorphous carbon phase decreased. This may be attributed to the high peak power density of the FS laser at higher power, which leads to direct ablation of the material, leaving less of the amorphous phase. Additionally, the hardness of a-Si, disordered carbon, and graphite produced by laser surface modification is lower than that of SiC, so their formation reduces the material's overall hardness. This reduction in hardness may also contribute to an improved material removal rate.

4. Discussion

The results indicate that laser surface modification introduces significant changes in ablation, roughness, oxidation, and composition. For the PS laser, the longer pulse duration distributes the laser energy over a more extended period, resulting in lower peak energy density and maximum temperature. This leads to smaller ablation depths, increased roughness, and slower material decomposition. However, the prolonged thermal effect promotes greater surface oxidation. In contrast, the FS laser, with its shorter pulse duration and higher peak energy density, which reduces the material ablation threshold, achieves larger ablation depths, and faster material decomposition. At high power, FS laser processing even directly ablates the surface, minimizing the accumulation of disordered carbon and graphite. These findings highlight that material ablation and decomposition are primarily governed by peak power density, while surface oxidation is more closely related to the duration of high-temperature conditions. Furthermore, as the power increases, the surface temperature of the material rises. A decrease in scanning speed and scanning interval causes the material surface to remain at high temperatures for a longer time. These factors collectively result in greater ablation depth, increased surface roughness, and enhanced surface oxidation.

The material changes induced by the above processes impact the material removal performance. Both the PS laser and FS laser generate LIPSS, which makes the surface structure more susceptible to damage. The fragility of the LIPSS increases with higher power levels. Additionally, oxidation and amorphous transformation occur on the surface, resulting in a reduction in hardness compared to the original material, thus lowering the overall surface hardness. These factors collectively enhance the material removal rate. When comparing the PS laser with the FS laser, the ablation depth is greater with the FS laser, but it results in lower surface quality and oxidation. Furthermore, under high power conditions, the degree of amorphous transformation is reduced. Therefore, the FS laser is more suitable for applications requiring a large ablation depth and minimal mechanical removal depth. On the other hand, the PS laser, which has lower ablation efficiency but provides higher surface quality and greater oxidation, is more appropriate for applications with a shallow ablation depth and substantial mechanical removal depth.

5. Conclusions

In this study, the effects of various laser parameters on the surface modification of SiC were investigated. The results demonstrate that, compared to the PS laser, the FS laser achieves significantly greater ablation depths and induces a more pronounced increase in surface roughness. In addition to pulse duration, other critical factors affecting ablation depth and surface roughness include laser power, scanning speed, and scanning interval. The PS laser leads to more substantial surface oxidation. Both PS and FS lasers result in the transformation of 4H-SiC into a-Si, disordered carbon, and graphite. These observations can be attributed to the higher peak energy density of the FS laser, which drives more intensive ablation, and the longer interaction duration of the PS laser, which enhances thermal effects. Overall, these findings provide valuable insights into the influence of laser parameters on the surface morphology and composition of SiC, providing a foundation for understanding laser-SiC interaction mechanisms and optimizing laser surface modification technique.

6. Acknowledgements

This work was mainly supported by the research studentship of The Hong Kong Polytechnic University (Project code: RMAN), the Research and Innovation Office of The Hong Kong Polytechnic University (Project code: 1-BECE) and the Research Grants Council of the Government of the Hong Kong Special Administrative Region (HKSAR), China (Project No. 15205423). In addition, the authors would like to express their sincere thanks for the funding support from the Innovation and Technology Commission (ITC) of HKSAR, China (MHP/151/22) and funding support from the State Key Laboratory of Ultra-Precision Machining Technology (Project code: BBX5).

References

[1] Wang W, Lu X, Wu X, Zhang Y, Wang R, Yang D, Pi X 2023 Adv Materials Inter **10** 2202369.
[2] Zhang X, Wang C, Cheung B C F, Mi G, Wang C 2024 Journal of the American Ceramic Society **107** 3724–3734.
[3] Xiong L, Wang C, Wu W, Xu L, Wang C, Deng H, Cheung B C F 2024 Surfaces and Interfaces **46** 104023.
[4] Liu H, Li Z, Zhang P, Zuo D, Xie W 2024 Applied Surface Science 160722.
[5] Chen P, Chi Z, Pan R, Qin F, Qiu P, Huang J, Xu S 2023 Journal of Materials Processing Technology **321** 118108.
[6] Xie X, Peng Q, Chen G, Li J, Long J, Pan G 2021 Ceramics International **47** 13322–13330.
[7] Chen G, Li J, Long J, Luo H, Zhou Y, Xie X, Pan G 2021 Applied Surface Science **536** 147963.
[8] Chen Y, Liu H, Cheng C, Chen C 2022 Appl. Phys. A **128** 1094.
[9] Yan Z, Mei X, Wang W, Fan Z, Pan A, Zheng Q 2025 Optics & Laser Technology **181** 111976.
[10] Bonse J, Gräf S 2020 Laser & Photonics Reviews **14** 2000215.
[11] Rehman Z U, Janulewicz K A 2016 Applied Surface Science **385** 1–8.
[12] Zhang R, Huang C, Wang J, Wang Q, Feng S, Zhao W, Tang A 2024 Ceramics International **50** 1193–1204.